Selective antibiofilm properties and biocompatibility of nano-ZnO and nano-ZnO/Ag coated surfaces

M. Rosenberg*[1, 2], M. Visnapuu[3], H. Vija[1], V. Kisand[3], K. Kasemets[1], A. Kahru[1, 4], A. Ivask[1, 5]

[1] Laboratory of Environmental Toxicology, National Institute of Chemical Physics and Biophysics, Tallinn, Estonia
[2] Department of Chemistry and Biotechnology, Tallinn University of Technology, Tallinn, Estonia
[3] Institute of Physics, University of Tartu, Tartu, Estonia
[4] Estonian Academy of Sciences, Tallinn, Estonia
[5] Institute of Molecular and Cell Biology, University of Tartu, Tartu, Estonia

* rosenbergmerilin@gmail.com

ABSTRACT

Spread of pathogenic microbes and antibiotic-resistant bacteria in health-care settings and public spaces is a serious public health challenge. Materials and surface-treatments that prevent solid surface colonization and biofilm formation or impede touch-transfer of viable microbes could provide means to decrease pathogen transfer from high-touch surfaces in critical applications. Both, ZnO and Ag nanoparticles have shown a great potential in antimicrobial applications. Although antimicrobial properties of such nanoparticle suspensions and their biocompatibility with human cells are well studied, less is known about nano-enabled solid surfaces. Here we demonstrate that surfaces coated with nano-ZnO or nano-ZnO/Ag composites possess species-selective medium-dependent antibiofilm activity against *Escherichia coli*, *Staphylococcus aureus* and *Candida albicans*. Colonization of nano-ZnO surfaces by *E. coli* and *S. aureus* was decreased in oligotrophic (nutrient-poor, no growth) conditions with *E. coli* showing higher sensitivity to Ag and *S. aureus* to Zn, respectively. Minor to no effect was observed for bacteria in growth medium (nutrient-rich, exponential growth). Inversely, compared to uncoated surfaces, nano-ZnO surfaces enhanced biofilm formation by *C. albicans* in oligotrophic conditions and just a minor transient negative effect was seen in nutrient-rich medium. However, enhanced *C. albicans* biofilm formation on nano-ZnO surfaces was effectively counteracted by the addition of Ag. Our results not only showed that nano-ZnO/Ag coated solid surfaces have the potential to effectively decrease surface colonization by the bacteria *E. coli* and *S. aureus* but also indicated the importance of the use of application-appropriate test conditions and exposure medium in antimicrobial surface testing. Possible selective enhancement of biofilm formation by the yeast *C. albicans* on Zn-enabled surfaces should be taken into account in antimicrobial surface development.

INTRODUCTION

Biofilms are by far the preferred lifestyle of bacteria [1], mostly in diverse nutrient-limited environmental niches. Biofilm communities cause biomass buildup on solid surfaces that results in major expenses in

marine traffic, water systems maintenance and in various industrial settings. Biofilms can also harbor potential human pathogens in food industry, health-care facilities, drinking water systems and on high-touch surfaces in public spaces. It is estimated that hard to treat pathogenic biofilms account for over 80% of all human microbial infections [2] with antibiotic-resistant ESKAPE pathogens [3] being the most problematic in the field. Biofilms pose a major medical challenge as they can be over 1000-fold more tolerant to antibiotics than their planktonic counterparts [4]. Spatially heterogeneous natural selection in biofilm milieu also contributes to antibiotic resistance development and transfer [5], [6] as well as producing antibiotic-resistant bacteria that are more fit and not easily outcompeted in the absence of the drug [7].

Controversially, most of the methods used to assess antimicrobial properties of surface materials, irrespective of their proposed application, either use planktonic cultures or study indirect effects such as release of antimicrobial compounds from the surfaces [8]. Such methods might not correctly report surface efficacy in proposed applications. Even if biofilm formation on material of interest is studied, often-used methods of biofilm viability assessment are prone to critical failures. For example, viability staining with propidium iodide and suitable counterstains can dramatically underestimate viability in both oligotrophic [9] and growth medium biofilms [10] while colony counts, the gold standard of microbiology, depend on viable cell harvesting efficiency and dispersion of harvested aggregates prior to cultivation [11], [12].

Susceptibility to metal ions has been demonstrated to be similar for both biofilms and planktonic cultures [13] which makes antimicrobial metal-based approaches good candidates to prevent biofilm formation on high-touch surfaces. Silver and copper are good examples historically used in infection prevention and marine antifouling even before deeper knowledge of microbes or biofilms was established. Another promising way is the development of antimicrobial surfaces containing photocatalysts that not only induce microbial killing but also degradation of organic matter under specific illumination conditions that could hopefully decrease dry touch-transfer of pathogens or delay moist surface colonization between light exposures. The most popular photocatalyst is TiO_2 but also ZnO is widely used [14]. In one of our previous studies [15] we demonstrated that in addition to killing bacterial cells during photocatalysis, TiO_2 surfaces also caused photooxidation of bacterial debris thus, referring to the possibility of extended efficacy of those surfaces.

The idea behind photodegradation is that light with high enough energy to exceed band gap energy of the photocatalytic metal oxide (e.g. 3.37 eV in the case of ZnO) will excite electron-hole pairs. The photogenerated electrons (e^-) and holes (h^+) can reduce or oxidize compounds like surface adsorbed O_2 and H_2O to produce reactive oxygen species (ROS). The produced ROS (e.g. superoxide anion radical $^{\bullet}O_2^-$

and hydroxyl radical $^{\bullet}OH$) are able to partially or completely degrade organic contaminants including microbes. It has been claimed that ZnO can produce ROS even without light activation [16] - ROS production via releasing of trapped electrons, so called "photocatalysis in the dark" [17]. Therefore, not only metal ions but assumingly also ROS can contribute to the antimicrobial and self-cleaning nature of photocatalytic metal oxide based surfaces in dark conditions. Increased antimicrobial and antibiofilm behavior of nano-ZnO covered dental implant [18] and ZnO thin film covered food-packaging polymer [19] compared to uncoated controls indicate a promising potential of ZnO-based coatings. The use of nanoparticle-based surfaces increases the potential efficiency and reactivity of such surfaces due to increased specific surface area of nanosized matter.

We have previously reported developing novel multi-effective antimicrobial coatings based on nano-ZnO/Ag composite particles [20]. The novelty of these coatings rises from a combined and complex effect of different antimicrobial mechanisms: (i) antimicrobial activity of Zn^{2+} ions, (ii) antimicrobial activity of Ag^{+} ions, and (iii) antimicrobial activity of ROS, generated at the surface of nano-ZnO and nano-ZnO/Ag via photocatalytic processes under UV-A illumination. Our coatings also have two additional advantages (i) degradation of organic debris (incl. dead bacteria) by ROS takes place on the surface and (ii) photocatalytic activity of ZnO is enhanced by the formation of nano-ZnO/Ag composite particles (via charge separation process in ZnO/Ag system).

Antimicrobial properties of our previously developed UV-A-induced nano-ZnO and nano-ZnO/Ag composite coated surfaces were evaluated using modified ISO 22196/27447 protocol and the nano-ZnO-enabled surfaces were found to be highly effective under UV-A illumination with over 3 log decrease in planktonic *E. coli* and *S. aureus* viability during 1 h exposure. Photodepositing Ag onto the nano-ZnO increased its photocatalytic activity and acted as an additional antimicrobial agent in the absence of UV-A exposure. [20]

With the intent to further develop these materials for use on high-touch surfaces in the public spaces, in this study we additionally assessed the efficacy of the surface materials against biofilm formation in application-appropriate oligotrophic environment and in the absence of UV-A exposure. For that we opted for a static model to grow biofilms directly on the studied surfaces and to be able to monitor dissolution-driven toxicity to the planktonic cells in a small closed system. A mixed approach combining physical methods (vortexing and ultrasonication) with chemical ones (addition of surfactant, using high salt concentration) was used for biofilm harvesting. Biocompatibility of the surfaces was studied using *in vitro* skin-relevant human cell growth directly on the nano-enabled surfaces.

RESULTS AND DISCUSSION

To assess anti-adhesion and metal release-associated antimicrobial properties of the coating materials, biofilm formation on the sparsely and densely coated nano-ZnO and sparsely coated nano-ZnO/Ag surfaces was studied. Biofilms were either grown in static oligotrophic environment (1:500 diluted nutrient broth in synthetic tap water, not supporting growth) at room temperature to mimic real-life-like use in moist environments (similar to previously used standard conditions for planktonic testing [20]) or in nutrient-rich growth mediums (LB, YPD; supporting exponential growth) resembling classical laboratory approach for studying biofilms [21]. *E. coli* MG1655 was used as a Gram-negative, *S. aureus* ATCC25923 as a Gram-positive and *C. albicans* CA14 as a human-relevant fungal model organism. The effect of the surfaces on biofilm formation was evaluated by harvesting viable adherent cells followed by colony counting or microscopy. In parallel, viability of planktonic cells above the surfaces was analyzed.

Bacterial biofilm formation on surfaces coated with nano-ZnO or nano-ZnO/Ag

Nano-ZnO inhibited bacterial biofilm formation in a dose-dependent manner in oligotrophic conditions (Fig. 1A, 1B) reaching maximum of 2.12 and 3.49 log reduction on dense nano-ZnO surface compared to uncoated surface after 72 h for *E. coli* and *S. aureus,* respectively. In growth medium, however, the dense nano-ZnO surface inhibited biofilm formation of *S. aureus* but not *E. coli* (Fig. 1D, 1E). Indeed, also the viability of planktonic *S. aureus* above the nano-ZnO surfaces was lower than that of *E. coli* (Fig. 2D and E). It was also evident that while there was rapid surface colonization taking place during the first 3 h of incubation in oligotrophic conditions, regardless of surface type, the surfaces in growth medium were either colonized more slowly or the initial adherence was weaker and adherent cells were more easily washed off during sample preparation.

Addition of Ag to the sparse nano-ZnO surfaces had transient negative effect on *E. coli* biofilm formation in oligotrophic conditions with an additional 0.5-1.6 log reduction in harvested viable cells (3-48 h post-inoculation, respectively) compared with sparse nano-ZnO without added Ag (Fig. 1A). This additional reduction decreased to a non-significant 0.34 log by 72 h. Ag had only a small but statistically significant effect on *S. aureus* biofilm formation in oligotrophic conditions (<0.5 log additional reduction compared to sparse nano-ZnO) indicating better tolerance to silver compared to *E. coli* (Fig. 1B).
As expected, addition of Ag to nano-ZnO surfaces had no effect on bacterial biofilm formation in organic-rich growth medium (Fig. 1D, 1E) due to lower bioavailability of silver.

In organics-rich growth mediua most of the Zn deposited on the nano-ZnO coated surfaces (Fig. 3, A-C) was released into the medium already after 24 h whereas in oligotrophic conditions up to 10 times less Zn was released (Fig. 3, D-F). Increased Zn release in growth media can be attributed to both, culture

acidification and formation of protein complexes driving Zn dissolution from nano-ZnO [22]–[24]. Higher release of Zn into microbial growth media yielded in lower toxicity to planktonic cells while in oligotrophic conditions more nano-ZnO remained on the surface resulting in both more effective inhibition of biofilm formation and lower planktonic viability.

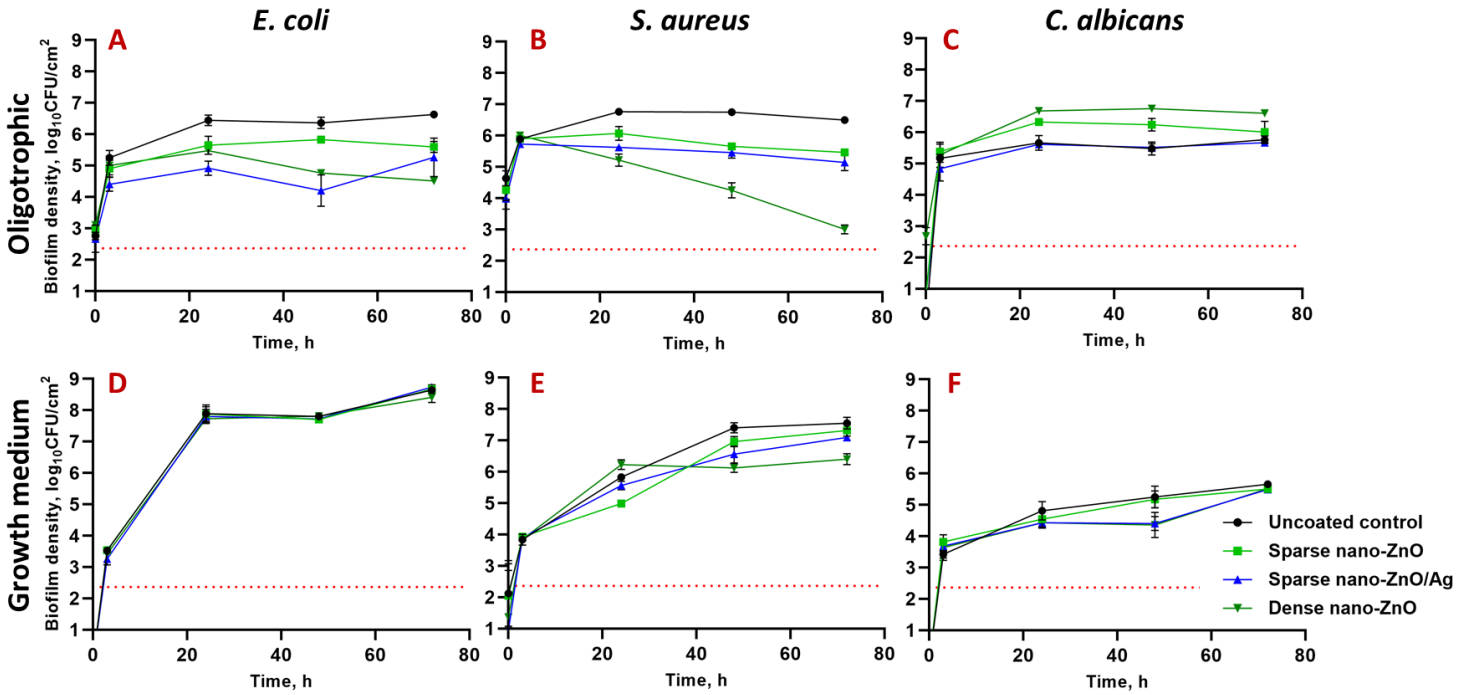

Figure 1. *E. coli* MG1655 (A, D), *S. aureus* ATCC25923 (B, E) or *C. albicans* CA14 (C, F) monospecies biofilms harvested at different time points from nano-ZnO or nano-ZnO/Ag or uncoated surfaces in static oligotrophic environment (1:500 diluted NB in synthetic tap water; A, B, C) or growth medium (LB: D, E; YPD: F). Biofilm formation was more affected by the nano-enabled coatings in oligotrophic environment than in growth medium with significantly decreased colonization by *E. coli* and *S. aureus* from 24 h onwards while nano-ZnO surfaces selectively enhanced surface colonization by *C. albicans*. Only dense nano-ZnO surfaces demonstrated statistically significant moderate colonization inhibiting effect on *S. aureus* in growth medium 48-72 h post-inoculation. Red dotted line represents the limit of quantification (231 CFU/cm^2). Data represents mean±SD of 3 independent experiments with 6-9 data points ±SD.

Slight decrease in overall planktonic viable counts at 3 h (Fig. 2, A-F) can be explained by microbial attachment to solid surfaces, including on the polystyrene well surface which decrease planktonic counts in oligotrophic conditions and is not yet compensated by proliferation during 3 h in growth medium at room temperature.

Zinc release from the dense nano-ZnO surface (Fig. 3) had a small but statistically significant negative effect of 0.63 logs reduction by 72 h on planktonic *E. coli* viability in oligotrophic conditions and no effect in growth medium (Fig. 2A, 2D) while the same surfaces decreased *S. aureus* planktonic viability in a dose-dependent manner in both oligotrophic conditions and growth medium (Fig. 2B, 2E) with maximum of 2.37 and 1.69 logs reduction, respectively. This effect can likely be attributed to relative sensitivity of *S.*

aureus towards Zn. Ag from sparse nano-ZnO/Ag had no significant effect on planktonic viability in growth medium (Fig. 2D, 2E) which can be explained by lower bioavailability of released Ag^+ ions due to complexing proteins and chloride in the medium [25]–[27].

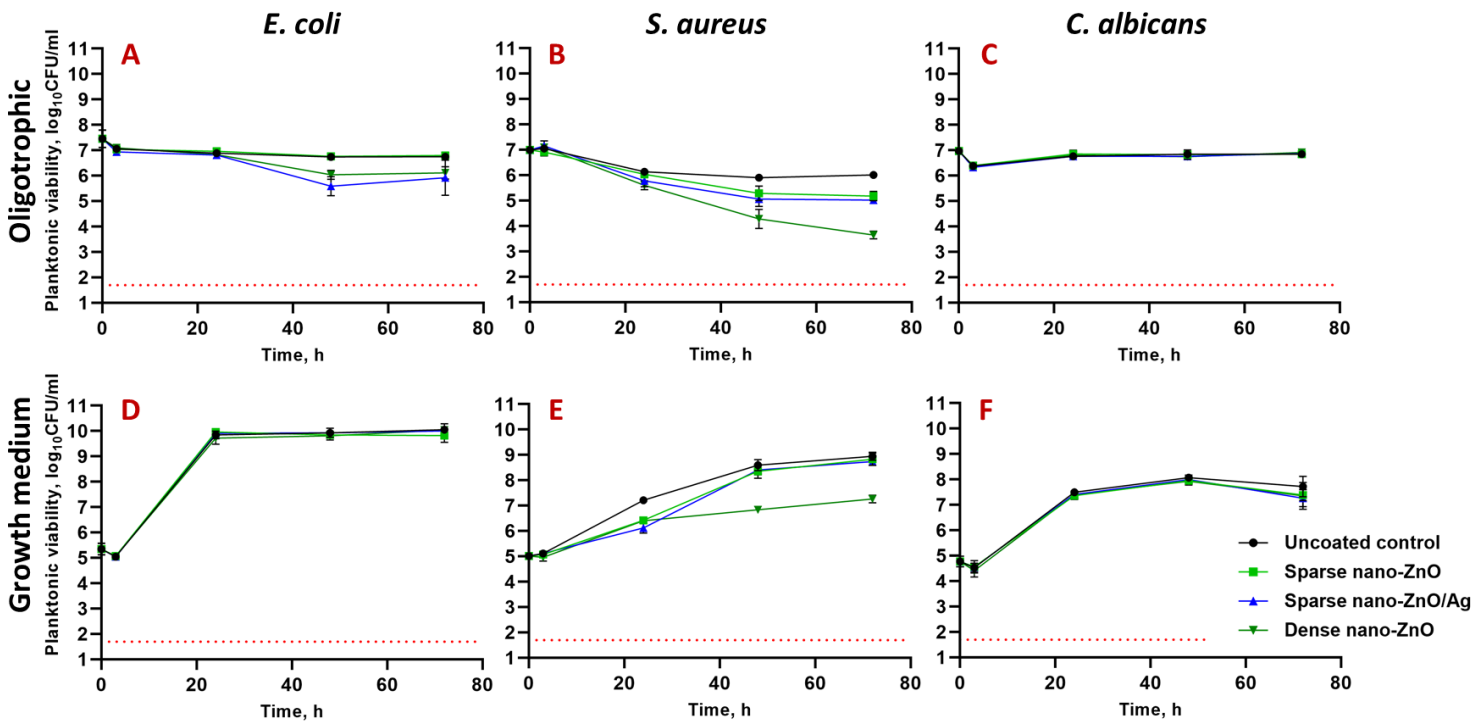

Figure 2. Viability of *E. coli* MG1655 (A, D), *S. aureus* ATCC25923 (B, E) or *C. albicans* CA14 (C, F) planktonic cells above nano-ZnO, nano-ZnO/Ag or uncoated surfaces in static oligotrophic environment (1:500 diluted nutrient broth in synthetic tap water; A, B, C) or growth medium (LB: D, E; YPD: F). Planktonic cells were generally more affected by nano-enabled coatings in oligotrophic environment than in growth medium. Red dotted line represents the limit of quantification (50 CFU/ml). Data represents mean±SD of 3 independent experiments with 6-9 data points ±SD.

Ag from the nano-ZnO/Ag surfaces decreased planktonic viability of only *E. coli*, but not *S. aureus* in oligotrophic conditions (Fig. 2A, 2B) which is in concordance with our previous findings that *S. aureus* is more sensitive to Zn and *E. coli* more sensitive to Ag [20]. Maximum calculated Ag concentration in the test system in case of complete release of Ag from the surface coating was estimated to reach 15.27±2.21 ng/ml (Supplementary Table 1). Actual release could not be reliably measured possibly due to high adsorption of Ag to organic matter in the test medium and/or polystyrene well walls.

Although zinc is an essential micronutrient, it possesses a dose-dependent antibacterial activity in higher concentrations. Zn tolerance in non-physiological concentrations has been shown to depend on microbial species with *C. albicans* and *P. aeruginosa* being less sensitive to Zn toxicity than *E. coli* or *S. aureus* [22]. ZnO nanoparticles have been demonstrated to additionally damage bacterial cell membranes and downregulate genes associated with managing oxidative stress in *S. aureus* as well as upregulate genes

associated with cation efflux in *E. coli* and *P. aeruginosa* and inhibit biofilm formation by *E. coli*, *S. aureus* and *P. aeruginosa* [28]–[31] among other microbes. Biofilm-inhibiting properties of Zn-based applications

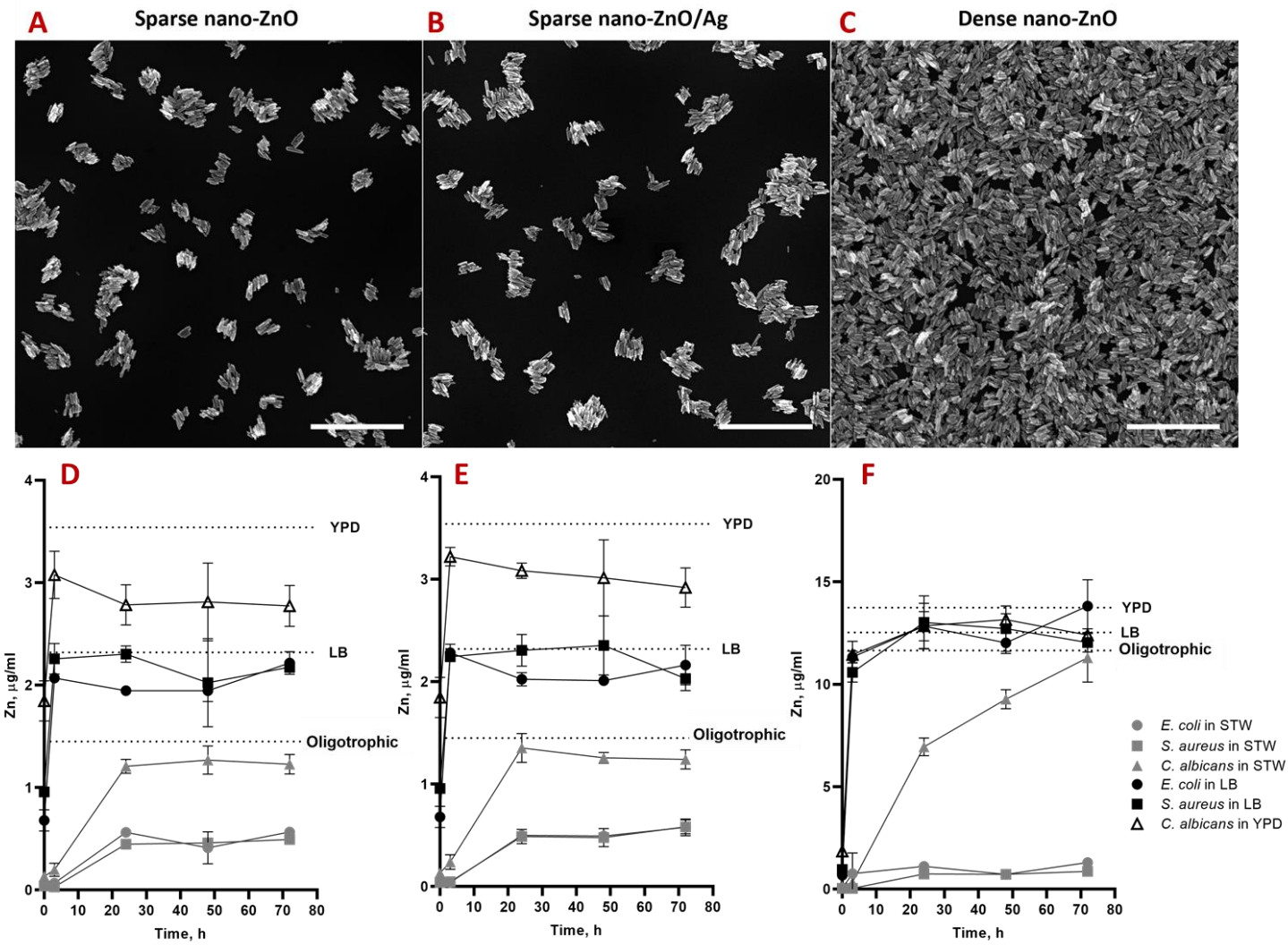

Figure 3. SEM images of sparse nano-ZnO (A), sparse nano-ZnO/Ag (B) and dense nano-ZnO (C) coated surfaces as well as measured Zn release from sparse ZnO (D), sparse ZnO/Ag (E) and dense ZnO (F) surface to the test environments (including the microbes) over time. A, B, C: scale bars represent 1 µm. D, E, F: maximum Zn concentration in each test environment (measured Zn background in different media + theoretical total Zn release from ZnO nanoparticles) is marked as a dotted line. Almost total Zn dissolution was reached already at 3 h in growth medium while dissolution equilibrium was much more slowly achieved in oligotrophic conditions and at lower Zn concentration (D-F). The only exception was *C. albicans* that significantly enhanced Zn release to near total dissolution in oligotrophic conditions. Data represents mean±SD of 3 independent experiments. Total Ag content of 23.56±3.42 ng/cm^2 in the sparse ZnO/Ag surface was measured which could result in up to 15.27±2.21 ng/ml concentrations in the 5 ml test volume (Supplementary Table 1).

can partially be attributed to general Zn toxicity to bacteria above physiological concentrations but also other biofilm-specific mechanisms of action could be involved. For example, it has been proposed that sublethal Zn concentrations could inhibit biofilm formation by interfering with quorum sensing [32]–[35].

Bacterial biofilm and cell morphology

Coverage of the surfaces by 48 h biofilm biomass in epifluorescence microscopy (Fig. 4) and higher magnification SEM images of representative microcolonies (Fig. 5) confirmed morphological and structural differences between biofilms grown on uncoated surfaces in growth medium and oligotrophic conditions as well as between biofilms on nano-ZnO coated and uncoated surfaces. Microscopy was chosen to be performed on 48 h fixed biofilm samples monostained with Syto 9 instead of viable biofilms stained with Syto 9 and propidium iodide (PI) because (i) based on pilot experiments, largest effect was expected at 48 h; (ii) PI is known to underestimates viability in biofilms [9], [10]; (iii) highly variable Syto 9 intensity in viable biofilms depending on viability state and Gram type of the cells [9], [36]; (iv) time limits of working with viable samples to achieve comparable representative results.

It must be noted, however, that adding liquid manipulation steps such as rinsing, fixation and gradual dehydration to the preparation of biofilms is likely to affect the appearance of biofilms and cause e.g., loss of biomass in each step. Kragh *et al.* have demonstrated that media removal and rinsing can critically affect quantitative biofilm analysis compared to undisturbed biofilms [10]. In addition, we observed that while oligotrophic bacterial biofilms retained their overall microcolony architecture during fixing and dehydration steps, biofilms formed in growth medium lost most of their biomass and surface coverage during dehydration steps prior to SEM. Taking into account also the rapid biofilm formation during the first 3 h in oligotrophic conditions (Fig. 1) we empirically suggest that biofilms formed in oligotrophic conditions are more strongly attached to the substratum.

In case of *E. coli*, also clear differences in cell surface structure were observed. *E. coli* biofilms in growth medium consisted of cells with smoother surfaces and less extracellular matrix (ECM) extended to solid surface while *E. coli* cells in oligotrophic biofilms had a more coarse surface structure and fibrillar ECM extended to solid surface. These differences occurred despite the fact that surface-associated amyloid fibers (SAFs) in the ECM were found to interconnect individual cells of *E. coli* (Supplementary Fig. 1-2) and *S. aureus* (Supplementary Fig. 3-4) biofilms in all growth and exposure conditions used. Although there was less *E. coli* biofilm on nano-ZnO-coated surfaces in oligotrophic conditions compared to uncoated surface (Fig. 1A, Fig. 4 upper panels) and cells tended to be shorter in length on nano-ZnO-coated surfaces, cells with normal morphology could be found even in direct contact with ZnO nanoparticles on dense nano-ZnO surfaces (Fig. 5, upper panels). ZnO nanoparticles were dissolved from the nano-ZnO surfaces in growth medium during 48 h incubation, as also confirmed by elemental analysis (Fig. 3F) and were not visible on SEM images (Fig. 5). Adherence of *S. aureus* cells to nanoparticles on dense nano-ZnO surfaces was also observed, although there were more damaged cells and blebbing occurring on nano-ZnO surfaces in oligotrophic conditions and on dense ZnO surface in growth medium compared to uncoated surfaces (Fig. 5, middle panels). Blebbing has been described not only for Gram-negative, but also for Gram-positive

bacteria and fungi [37] and appears to have a more general role in stress response, virulence and intercellular communication across the domains of life. Vesicle formation is also confirmed in case of *S. aureus* [38] and can take place for example in response to antibiotic stress thereby increasing virulence [39].

There were no clear morphological differences between *S. aureus* biofilm cells on uncoated surfaces in growth medium and oligotrophic conditions besides larger cell size in growth medium (Fig. 5, middle panels). Although Zn-enhanced cell-to-cell adherence has been described for *S. aureus* [40], [41], *S. aureus* tended to preferably form cell aggregates (cell-to-tell adherence) regardless of surface type while *E. coli* tended to cover surface (cell-to-surface adherence) and thereafter form biofilm in height.

We also hypothesized that Zn might interfere with bacterial surface-associated amyloid (SAF; [42]–[45]) formation as it can modulate fibrillar structure of other amyloids [46]–[50] and could thereby disrupt SAF-mediated surface colonization. Although cell surface morphology seemed to differ between *E. coli* cells grown on nano-ZnO and uncoated surfaces in oligotrophic conditions (Fig. 5, top panel), we found no major qualitative differences in amyloid staining of those biofilms (Supplementary Fig. 1-4). Qualitative results do not strictly rule out smaller Zn-dependent differences, which amyloid signal quantification could possibly discriminate, if present.

Yeast biofilm formation on surfaces coated with nano-ZnO or nano-ZnO/Ag

Nano-ZnO enabled surfaces promoted *C. albicans* biofilm formation in oligotrophic conditions with up to 1.27 log increase in viable attached cells at 48 h time point compared to uncoated surface (Fig. 1C) and viability of planktonic cells above the surfaces was not significantly affected regardless of medium used (Fig. 2C, 2F). Silver-containing surfaces had no significant effect on *C. albicans* biofilm formation nor on planktonic viability in oligotrophic conditions compared to uncoated surfaces. However, considering enhanced *C. albicans* biofilm formation on sparse nano-ZnO surfaces and biofilm formation on sparse nano-ZnO/Ag surfaces in oligotrophic conditions (Fig. 1C) demonstrating a significant 0.55-0.72 log reduction compared to sparse nano-ZnO surface during 3-48 h respectively, it could be concluded that silver transiently inhibited *C. albicans* biofilm formation bringing it down to control level. This inhibition was lost 72 h post-inoculation. No biofilm promoting effect was observed in growth medium where inversely a moderate transient biofilm inhibition on both sparse nano-ZnO/Ag (0.85 log decrease) and dense nano-ZnO (0.89 log decrease) surfaces was observed at 48 h (Fig. 1F). Inhibitory effect of silver is further illustrated by the presence of areas with several flattened “ghost cells” on sparse nano-ZnO/Ag surface in growth medium (Supplementary Fig. 5) accompanying slight decrease in biofilm cell count 48 h post-inoculation (Fig. 1F). Similar areas with dead cells were not observed in other conditions and seemed to serve as a matrix for the biofilm to grow on. Congo Red (CR), used to stain SAFs, also stains cellulose

and chitin in fungal cell walls [51] due to structural similarity to cellulose. In this study, we have used CR also to visualize *C. albicans* cells by staining both cell wall and fungal SAFs [52]. Regarding possible cellulose signal interfering with amyloid staining of *E. coli*, as cellulose is a known component in ECM of several *Enterobacteriaceae* species, it is known that *E. coli* K-12 strains, including MG1655 have a stop codon mutation in the cellulose operon and do not produce cellulose [53].

Pseudohyphal morphology of the dimorphic fungus *C. albicans* [54] was only observed in oligotrophic conditions, where yeast form was qualitatively more dominant on dense nano-ZnO surface (bottom panels in Fig. 4 and 5). No true hyphae were observed nor expected from this strain in the conditions used. In addition, Harrison *et. al* have demonstrated that sub-inhibitory Zn^{2+} concentrations can interrupt yeast to hyphal differentiation in *Candida* biofilms [55] and it has been suggested that zinc-responsive transcription factor Zap1 is a negative regulator of biofilm matrix accumulation and maturation [56] also directing the yeast-hypha balance to yeast form [57]. On the other hand, filamentation is not a prerequisite for biofilm formation [58] as can also be seen in our results.

Enhanced dose-dependent biofilm formation of *C. albicans* on nano-ZnO-coated surfaces in oligotrophic conditions cannot be explained by differences in the hydrophilic properties of nano-ZnO coated and uncoated surfaces (Supplementary Fig. 6). However, *C. albicans* has been demonstrated to possess systems to harvest extracellular Zn and store Zn intracellularly in zincosomes [59] which enables *C. albicans* to both overcome nutritional immunity in host organism as well as to detoxify Zn^{2+} excess. Active uptake of extracellular Zn could also be the reason, why nano-ZnO is depleted from the surfaces in oligotrophic conditions in the presence of *C. albicans* but not bacteria (Fig. 3, D-F). For dense nano-ZnO surfaces this effect was also clearly observable on SEM images (Fig. 5, right column). Interestingly, previously published results on zinc effects on *Candida* biofilm formation are contradictory. For example, Kurakado *et al.* demonstrated an increase in *C. albicans* biofilm formation as a response to $ZnSO_4$ and a decrease in response to zinc chelator [60] while several others report Zn-associated biofilm inhibition [61]–[63]. These contradictions could be partly due to different average and local Zn concentrations reached in these studies while we had the nano-ZnO attached to a solid surface resulting in lower average Zn concentration in the test environment or due to growth-related and physiological differences in various oligotrophic and nutrient-rich environments. In the light of existing and emergent drug-resistant *Candida* spp. [64] Zn-enhanced *C. albicans* biofilm formation in oligotrophic conditions should be studied further to reveal mechanistic causes of the biofilm-promoting phenomenon.

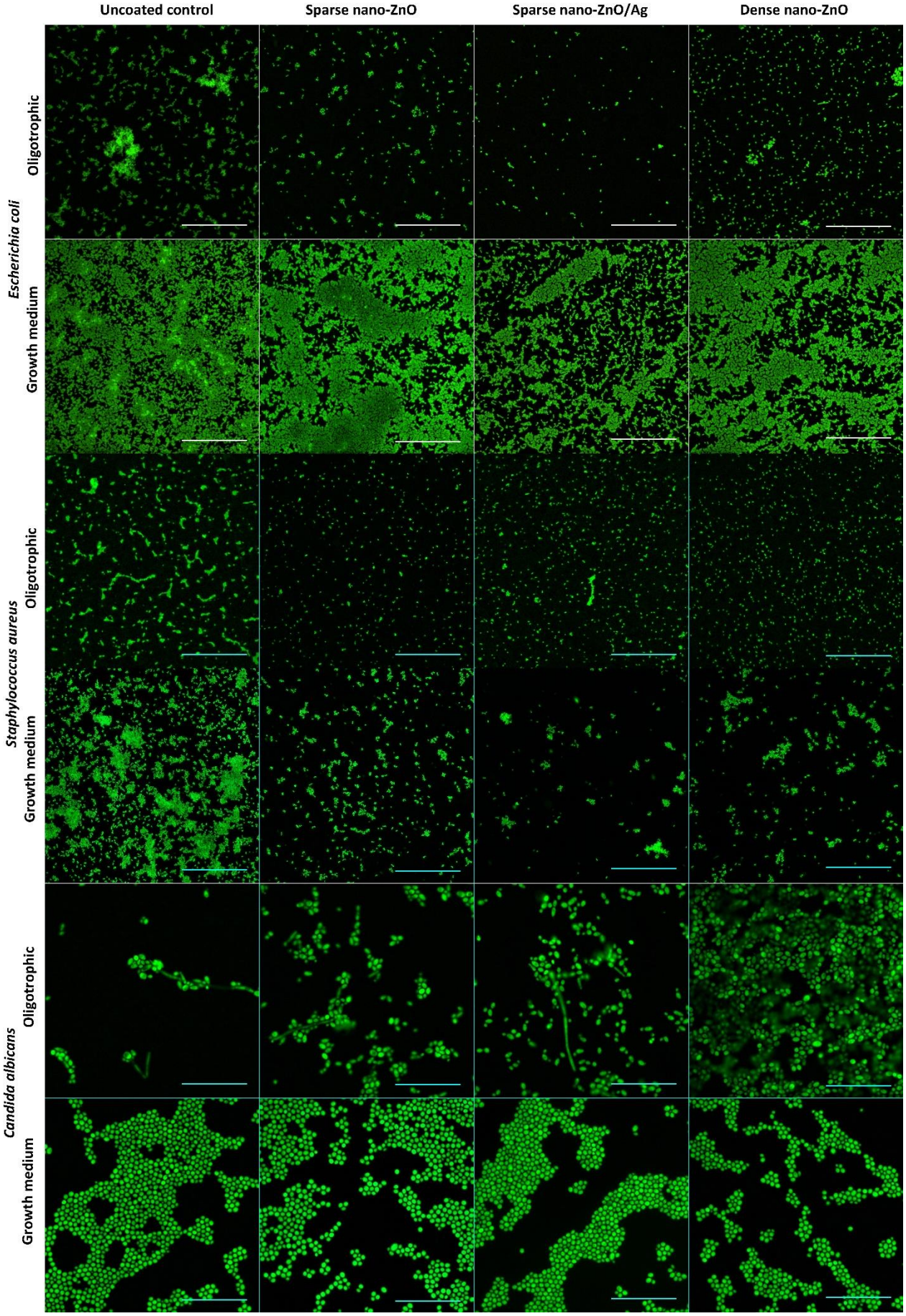

Figure 4. Representative epifluorescence images of *E. coli*, *S. aureus* or *C. albicans* 48 h biofilms on uncoated surfaces or on surfaces coated with nano-ZnO or nano-ZnO/Ag in oligotrophic conditions and growth medium. Fixed biofilms were stained with DNA- and RNA-binding Syto 9. Scale bars represent 50 µm.

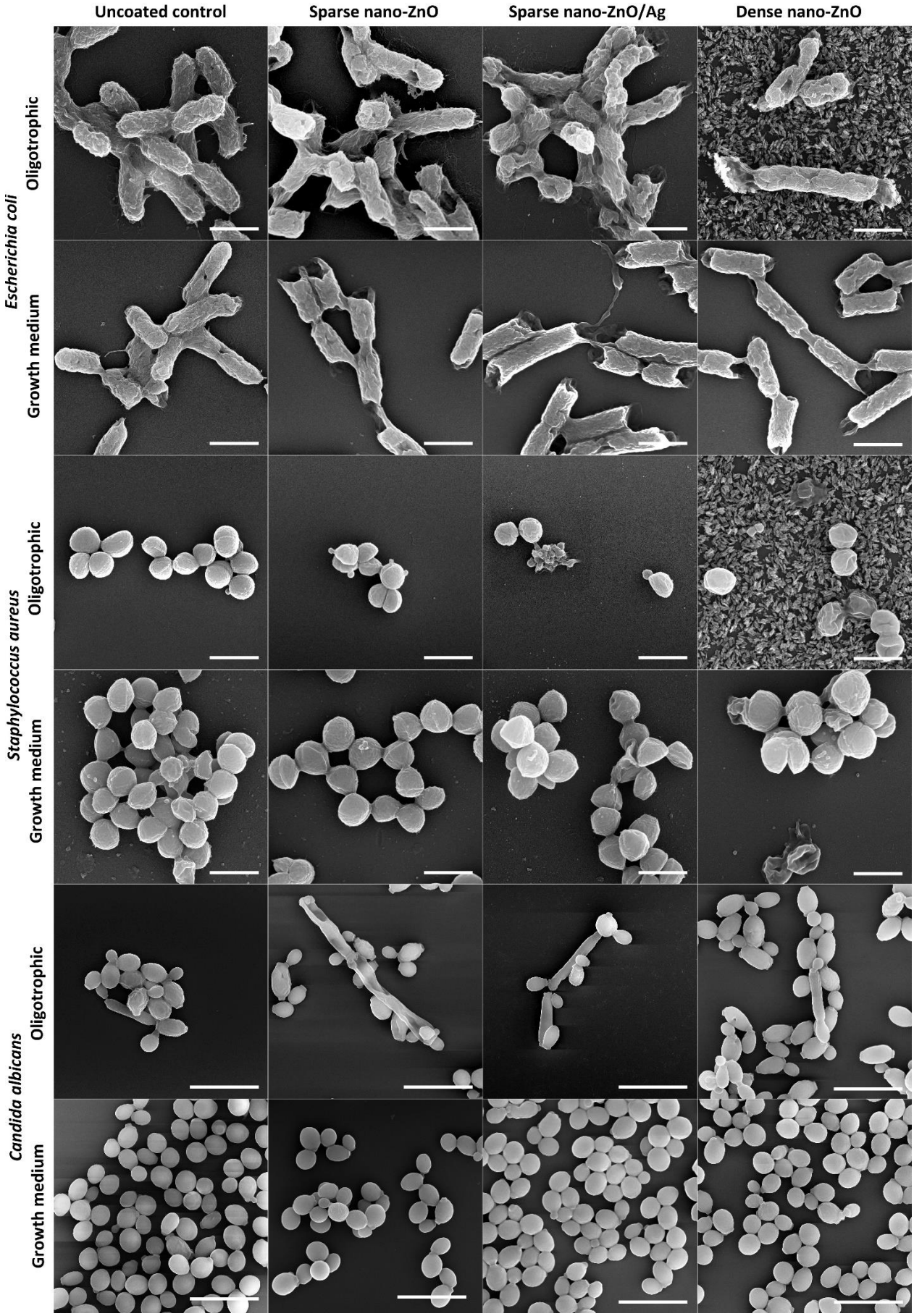

Figure 5. Characteristic SEM images of *E. coli*, *S. aureus* and *C. albicans* cell and microcolony morphology in 48 h biofilm aggregates on uncoated surfaces or on surfaces coated with nano-ZnO or nano-ZnO/Ag in oligotrophic conditions and growth medium. Scale bars represent 1 µm for bacteria and 10 µm for *C. albicans*. For designation of the surface coatings, see Fig. 3 (A-C).

In vitro biocompatibility of nano-ZnO and nano-ZnO/Ag surfaces

In order to assess the safety of nano-ZnO and nano-ZnO/Ag surfaces to human cells, the growth of human keratinocytes directly on the surfaces in standard cell culture conditions was evaluated. Normal confluency and morphology of human keratinocytes on nano-ZnO coated surfaces was observed (Fig. 6).

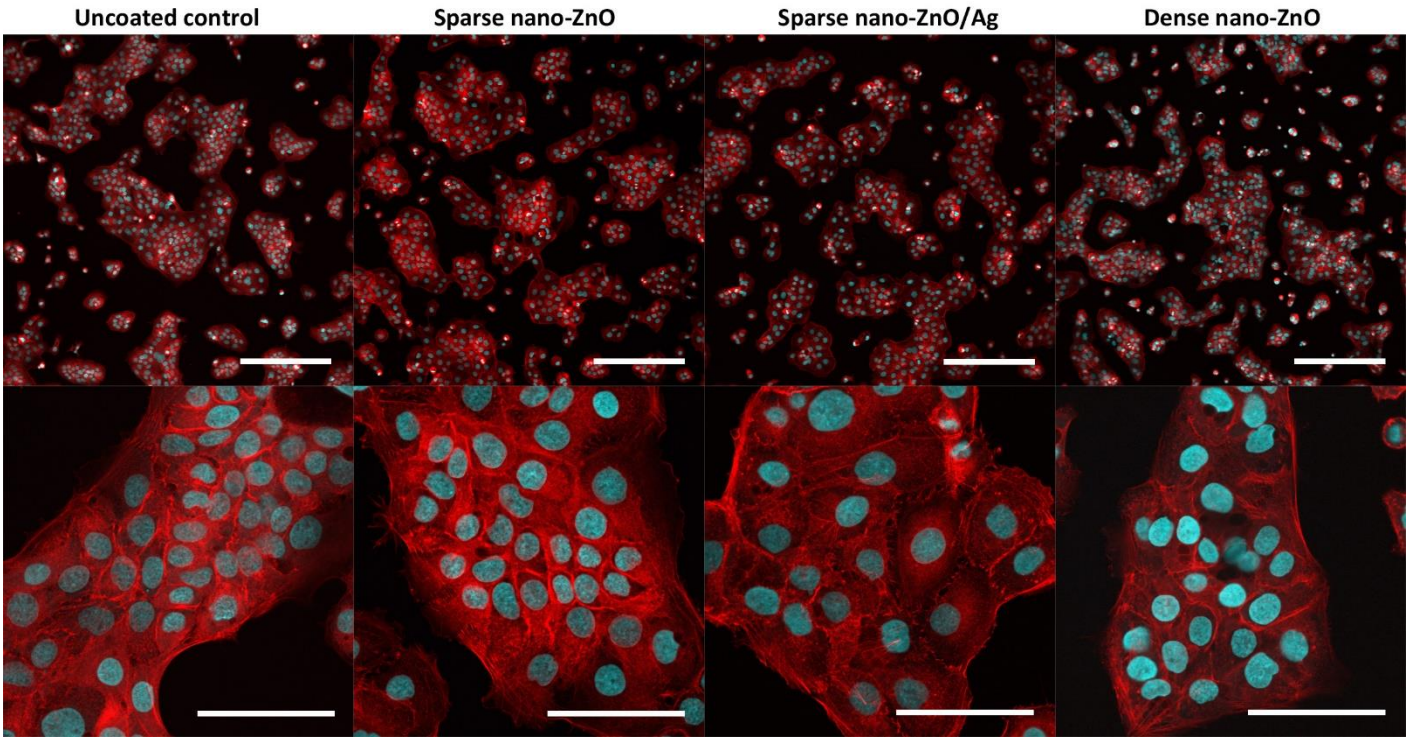

Figure 6. Representative confocal microscopy images of HaCaT keratinocytes on nano-ZnO or nano-ZnO/Ag coated surfaces: upper panel – lower magnification (scale bar 200 µm), lower panel – higher magnification (scale bar 50 µm); nuclei – cyan (Hoechst 33342), cytoskeleton – red (Phalloidin-TRITC). Cells are viable (Fig. 7) and appear normal on all surfaces.

Slightly enhanced attachment and growth of keratinocytes on dense nano-ZnO surfaces (Fig. 7) cannot be explained by differences in hydrophilicity of the different surfaces (see water contact angles on different surfaces in Supplementary Fig. 6). However, this observation is not unexpected as zinc is known to promote wound healing [65] and has been shown to also promote keratinocyte migration and proliferation as well as to modulate integrin expression needed for adherence to extracellular matrix [66]. Enhanced growth of human keratinocytes was observed despite the fact that there was enough Zn deposited on dense nano-ZnO surfaces to cause toxicity to the cells in case of total release into culture medium (Supplementary Fig. 7).

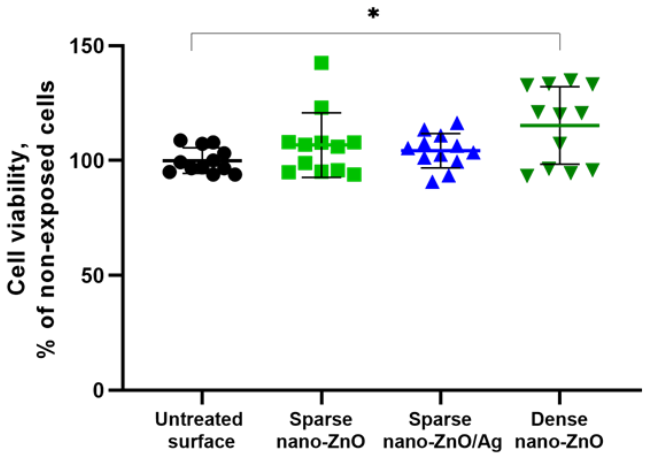

Figure 7. Cytotoxicity of nano-ZnO and nano-ZnO/Ag coated **surfaces to HaCaT keratinocytes grown directly on the surfaces** in standard cell-culture conditions (DMEM high glucose medium supplemented with Na-pyruvate (1mM), penicillin-streptomycin (100 U/mL;100 µg/mL), fetal bovine serum (10%), 37 °C, 5% CO2). No direct cytotoxicity of nano-enabled surfaces was observed. Increased growth of keratinocytes was observed on dense nano-ZnO surfaces. * denotes statistically significant difference (P<0.05)

SUMMARY

This study showed that in general, bacterial *E. coli* and *S. aureus* monospecies biofilm formation on nano-ZnO and nano-ZnO/Ag composite-enabled surfaces was inhibited in a dose-dependent manner: sparsely coated nano-ZnO surfaces were less inhibitory than densely coated ones. No significant inhibition of yeast biofilm was observed. On the contrary, enhancement of *C. albicans* biofilm formation was observed on densely coated nano-ZnO surfaces in oligotrophic conditions. This observation is certainly disadvantageous considering the emergence of drug-resistant infections of *Candida spp.* Interestingly, similar observation to *C. albicans* was done with human keratinocytes that were used to study the potential cytotoxicity of the surfaces. No inhibition of keratinocyte attachment and growth on nano-enabled surfaces was observed and on densely coated nano-ZnO surfaces, higher amount of viable keratinocytes was detected. Such selection could be favorable in attracting host cells in long-term implanted medical devices or promoting wound healing.

It is also important to highlight the role of the test environment. Except for Zn toxicity towards *S. aureus*, all above-mentioned antimicrobial and antibiofilm effects were detected only in oligotrophic environment and not in widely used microbial growth media. Moreover, selection of detection method proved critical in the quality of information acquired as biomass was lost in every liquid manipulation step and information such as colony counts or microcolony morphology and composition can significantly differ depending on sample preparation protocol. Media removal and washing steps have been shown to critically affect quantitative biofilm analysis. We add to that and propose that liquid manipulation steps can also easily introduce compositional biases (e.g. losing *C. albicans* “ghost cells”) or exaggerate biomass

differences as *E. coli* biofilm in growth medium was much more easily washed off the surfaces than biofilm formed in oligotrophic conditions.

METHODS

Surfaces

ZnO or ZnO/Ag nanoparticles were deposited on 18x18 mm square cover glasses (2855-18, Corning). Two different coating densities of nano-ZnO were used further referred to as sparse and dense, depicted on Fig. 3 (A-C). Nano-ZnO/Ag composite particles were used only in sparse coating density. Physical and chemical properties of the nanoparticles used as well photocatalytic and antibacterial activity of the surfaces used in this study have been previously described [20]. Total Zn content in the nano-coatings was analyzed using TXRF (S2 Picofox, Bruker) and Ag content with AAS (ContrAA 800, Analytic Jena AG) after 1 h treatment in 0.5 ml concentrated HNO_3. The results are shown in Supplementary Table 1.

Biofilm formation, harvesting and quantification

Monospecies biofilms of *E. coli* MG1655, *S. aureus* ATCC25923 and *C. albicans* CA14 were studied. Sterile nano-ZnO, nano-ZnO/Ag or uncoated surfaces were placed into non tissue culture treated 6-well polystyrene plate wells. 5 ml of microbial inoculum was added to each well. To prepare inoculums, overnight cultures of microbes were pelleted by centrifugation (7000 g, 10 min) and washed twice with deionized water before re-suspension in test medium and density optimization. Initial cell density was about 10^7 CFU/ml in oligotrophic conditions, i.e., synthetic tap water (STW; Table 1) containing 1:500 diluted nutrient broth (NB; Table 1) and 10^5 CFU/ml in growth media, i.e., lysogeny broth (LB, Table 1) in case of bacteria and yeast extract-peptone-dextrose medium (YPD, Table 1) in case of yeast. Surfaces were incubated in dark static conditions (covered with aluminum foil) at room temperature (22 ˚C) to allow biofilm formation. After 0, 3, 24, 48 and 72 h three samples of each surface were dip-rinsed in PBS (Table 1) with sterile forceps, carefully drained from one corner and submerged in 15 ml 0.5x neutralizing broth (SCDLP; Table 1) with 1.5M NaCl in 50 ml centrifuge tube, vortexed for 30 sec at max speed, ultrasonicated for 15 min in ultrasonic bath (Branson1800) and again vortexed for 30 sec. An aliquot of each resulting suspension was serially diluted in PBS and drop-plated on nutrient agar (NA) or yeast growth agar (YPD agar, Table 1) for colony counting. Planktonic fraction in 5 ml media over biofilms in from each well was mixed by pipetting, serially diluted and plated for planktonic colony count. To assess Zn release from the surfaces, an aliquot from planktonic fraction (including microbes) in wells above the biofilms was taken for elemental analysis. TXRF (S2 Picofox, Bruker) was used for Zn analysis. Maximum calculated Ag concentration in the test system in case of complete release of Ag from the surface coating was estimated

to reach 15.27±2.21 ng/ml (Supplementary Table 1). Actual release could not be measured due to high adsorption of Ag to organic material and well walls.

Biofilm and planktonic viable counts were calculated as follows:

$$\frac{\mathbf{CFU}}{\mathbf{cm^2}} = \text{CFUs counted} \times \text{serial dilution factor} \times \frac{\text{sonication volume (µl)}}{\text{plated volume (µl)}} \times \frac{1}{\text{sample surface area (cm}^2\text{)}}$$

$$\mathbf{CFU/ml} = \text{CFUs counted} \times \text{dilution factor} \times \frac{1000\ (\text{µl})}{\text{plated volume (µl)}}$$

Table 1. Media and buffers

Synthetic tap water (STW; DIN10531), prepared as 5x stock	300 mg/L $NaHCO_3$, 175 mg/L $MgSO_4$, 300 mg/L $CaCl_2$; pH 7.5 in 1xSTW
Nutrient broth (ISO 22196)	3 g/L meat extract, 10 g/L peptone, 5 g/L NaCl; pH 6.8-7.2
Lysogeny broth (LB)	5g/L tryptone, 5 g/L yeast extract, 5 g/L NaCl; pH 6.8-7.2
Yeast extract peptone dextrose medium (YPD) and respective agar	20 g/L peptone, 10 g/L yeast extract, 20 g/L glycose + 15 g/L agar for plates; pH 6.8-7.2
Phosphate buffered saline (PBS)	8 g/L NaCl, 0.2 g/L KCl, 0,81 g/L, Na_2HPO_4x2H_2O, 0.2 g/L KH_2PO_4; pH 7.1
Nutrient agar (ISO 22196)	5 g/L meat extract, 10 g/L peptone, 5 g/L NaCl, 15 g/L agar; pH 7.0-7.2
Soybean casein digest broth with lecithin and polyoxyethylene sorbitan monooleate (SCDLP broth; ISO 22196)	17 g/L casein peptone, 3 g/L soybean peptone, 5 g/L NaCl, 2.5 g/L Na_2HPO_4, 2.5 g/L glucose, 1.0 g/L lecithin, 7.0 g/L nonionic surfactant; pH 6.8-7.2
Sodium cacodylate buffer, prepared as 0.2 M stock	4.8 g $Na(CH_3)_2AsO_2$ x 3 H_2O in 100 ml deionized water brought to pH 7.4 with the addition of 5.6 ml 0.2M HCl

Ultrasonication protocol

SCDLP (Table 1) was used for toxicity neutralizing properties (ISO 27447) and its surfactant content was expected to enhance releasing biofilms from surfaces. 1.5M NaCl was used to aid in biofilm harvesting as

it has also been successfully used for extracellular matrix removal [67] and does not influence microbial viability when combined with ultrasonication and vortexing (Supplementary Fig. 8). Staining with 30 µM propidium iodide and 5 µM Syto 9 with subsequent epifluorescence microscopy (see below) was used to evaluate biofilm harvesting efficiency. It was confirmed that adherent cells were removed from the surfaces (data not shown).

Staining and microscopy

Biofilms were stained to visualize total cellular biomass (DNA/RNA), surface-associated amyloid fibers (SAF) and chitin (in case of yeast). Before staining, the biofilms were dip-rinsed in PBS (Table 1) to remove loosely bound cells as described above and fixed by 2-h incubation in 2.0% glutaraldehyde in 0.1M sodium cacodylate buffer (Table 1) followed by rinsing once in the same buffer. For total cellular biomass visualization, nucleic acids were stained by incubating the fixed cells for 15 min with 5 µM Syto9. For staining of SAF and chitin (fungal cell wall component), fixed biofilms were incubated for 15 min with 5 µM Syto9 and 10 µM Congo Red. Stained biofilms were visualized with Olympus CX41 using exciter filter BP475, dichroic mirror DM500, barrier filter O515IF (Syto9 staining) or with Zeiss LSM800 confocal laser scanning microscope (CLSM) using excitation/emission track settings of 488 nm/505-550 nm (Syto9) and 561 nm/575-700 nm (Congo Red).

To visualize biofilm morphology, electron microscopy was used. For that, fixed biofilms were gradually dehydrated with ethanol, air-dried, coated with 3 nm Au/Pd layer (Polaron Emitech SC7640 Sputter Coater) and visualized with scanning electron microscopy (FEI Helios NanoLab 600).

Cytotoxicity testing

Toxicity of the surfaces was tested on human immortalized HaCaT keratinocytes (ThermoFisher). Cells were maintained in DMEM high glucose medium supplemented with Na-pyruvate (1mM), penicillin-streptomycin (100 U/mL and 100 µg/mL, respectively) and fetal bovine serum (10%) at 37 °C and 5% CO_2. During maintenance, the cell density was kept between 0.5-1x10^6 cells/ml. Each type of surface in four replicates was placed into a separate well of a 6-well plate and 2 ml of cell suspension (4*10^4 cells/mL) in supplemented DMEM medium was added. Cells were cultivated for 48 h, surfaces were removed using tweezers to a new well of a 6-well plate. One replicate of each type of surface was left for microscopy while to the rest of three replicates 0.33% of Neutral Red (Sigma) solution in supplemented DMEM medium was added and incubated at 37 °C and 5% CO2 for 4 hours. After that, the dye solution was removed by double washing with PBS and the dye remaining within viable cells was dissolved over 10 min (gentle shaking) using 1 ml of Neutral Red Assay Solubilization Solution (Sigma). The intensity of Neutral Red dye was measured spectrophotometrically at 540 nm using Fluoroskan plate reader (Thermo). Cell viability on nano-ZnO and nano-ZnO/Ag surfaces was calculated as percentage of viability on uncoated

surface. Cell viability assays on surfaces were repeated twice. For microscopy, the surfaces with cells were first covered with 3.7% formaldehyde in 0.1% TritonX-100 solution for 10 min, then with 1 µg/ml solution of Hoechst 33342 (ThermoFisher) and 1 µg/ml Phalloidin-TRITC (Sigma) in PBS for 30 min. After that, the dye solution was removed and cells were imaged using confocal microscope with filter settings for DAPI and TRITC.

For cytotoxicity assays of respective soluble salts (Supplementary Fig. 7), exposure to HaCaT cells was carried out in 96-well format and cell viability was assessed using Neutral Red assay, essentially as described above.

Statistical analysis

One- or two-way ANOVA analysis followed by Tukey *post-hoc* test was used to detect significant differences in multiple comparisons at 0.05 significance level using GraphPad Prism 8.3.0. Log-transformed data was used for the analysis of CFU counts. Only statistically significant ($P<0.05$) differences and log reductions are mentioned in the text unless stated otherwise.

REFERENCES

[1] H.-C. Flemming and S. Wuertz, “Bacteria and archaea on Earth and their abundance in biofilms,” *Nature Reviews Microbiology*, vol. 17, no. 4, pp. 247–260, Apr. 2019, doi: 10.1038/s41579-019-0158-9.

[2] NIH, “Research on microbial biofilms: PA Number: PA-03-047,” National Institute of Health, Dec. 2002.

[3] J. N. Pendleton, S. P. Gorman, and B. F. Gilmore, “Clinical relevance of the ESKAPE pathogens,” *Expert Review of Anti-infective Therapy*, vol. 11, no. 3, pp. 297–308, Mar. 2013, doi: 10.1586/eri.13.12.

[4] H. Ceri, M. E. Olson, C. Stremick, R. R. Read, D. Morck, and A. Buret, “The Calgary Biofilm Device: new technology for rapid determination of antibiotic susceptibilities of bacterial biofilms,” *J. Clin. Microbiol.*, vol. 37, no. 6, pp. 1771–1776, Jun. 1999.

[5] M. T. France, A. Cornea, H. Kehlet-Delgado, and L. J. Forney, “Spatial structure facilitates the accumulation and persistence of antibiotic-resistant mutants in biofilms,” *Evol Appl*, vol. 12, no. 3, pp. 498–507, Mar. 2019, doi: 10.1111/eva.12728.

[6] I. Olsen, “Biofilm-specific antibiotic tolerance and resistance,” *Eur J Clin Microbiol Infect Dis*, vol. 34, no. 5, pp. 877–886, May 2015, doi: 10.1007/s10096-015-2323-z.

[7] A. Santos-Lopez, C. W. Marshall, M. R. Scribner, D. J. Snyder, and V. S. Cooper, “Evolutionary pathways to antibiotic resistance are dependent upon environmental structure and bacterial lifestyle,” *Elife*, vol. 8, 13 2019, doi: 10.7554/eLife.47612.

[8] J. Sjollema *et al.*, “In vitro methods for the evaluation of antimicrobial surface designs,” *Acta Biomaterialia*, vol. 70, pp. 12–24, Apr. 2018, doi: 10.1016/j.actbio.2018.02.001.

[9] M. Rosenberg, N. F. Azevedo, and A. Ivask, “Propidium iodide staining underestimates viability of adherent bacterial cells,” *Scientific Reports*, vol. 9, no. 1, Dec. 2019, doi: 10.1038/s41598-019-42906-3.

[10] K. N. Kragh, M. Alhede, L. Kvich, and T. Bjarnsholt, “Into the well—A close look at the complex structures of a microtiter biofilm and the crystal violet assay,” *Biofilm*, p. 100006, Sep. 2019, doi: 10.1016/j.bioflm.2019.100006.
[11] K. D. Mandakhalikar, J. N. Rahmat, E. Chiong, K. G. Neoh, L. Shen, and P. A. Tambyah, “Extraction and quantification of biofilm bacteria: Method optimized for urinary catheters,” *Sci Rep*, vol. 8, no. 1, p. 8069, Dec. 2018, doi: 10.1038/s41598-018-26342-3.
[12] H. Kobayashi, M. Oethinger, M. J. Tuohy, G. W. Procop, and T. W. Bauer, “Improved detection of biofilm-formative bacteria by vortexing and sonication: a pilot study,” *Clin. Orthop. Relat. Res.*, vol. 467, no. 5, pp. 1360–1364, May 2009, doi: 10.1007/s11999-008-0609-5.
[13] J. J. Harrison, H. Ceri, C. A. Stremick, and R. J. Turner, “Biofilm susceptibility to metal toxicity,” *Environ Microbiol*, vol. 6, no. 12, pp. 1220–1227, Dec. 2004, doi: 10.1111/j.1462-2920.2004.00656.x.
[14] A. Sirelkhatim *et al.*, “Review on Zinc Oxide Nanoparticles: Antibacterial Activity and Toxicity Mechanism,” *Nano-Micro Lett.*, vol. 7, no. 3, pp. 219–242, Jul. 2015, doi: 10.1007/s40820-015-0040-x.
[15] U. Joost *et al.*, “Photocatalytic antibacterial activity of nano-TiO2 (anatase)-based thin films: Effects on Escherichia coli cells and fatty acids,” *Journal of Photochemistry and Photobiology B: Biology*, vol. 142, pp. 178–185, Jan. 2015, doi: 10.1016/j.jphotobiol.2014.12.010.
[16] V. Lakshmi Prasanna and R. Vijayaraghavan, “Insight into the Mechanism of Antibacterial Activity of ZnO: Surface Defects Mediated Reactive Oxygen Species Even in the Dark,” *Langmuir*, vol. 31, no. 33, pp. 9155–9162, Aug. 2015, doi: 10.1021/acs.langmuir.5b02266.
[17] H. Sun *et al.*, “Zinc oxide/vanadium pentoxide heterostructures with enhanced day-night antibacterial activities,” *Journal of Colloid and Interface Science*, vol. 547, pp. 40–49, Jul. 2019, doi: 10.1016/j.jcis.2019.03.061.
[18] E. H. Abdulkareem, K. Memarzadeh, R. P. Allaker, J. Huang, J. Pratten, and D. Spratt, “Anti-biofilm activity of zinc oxide and hydroxyapatite nanoparticles as dental implant coating materials,” *Journal of Dentistry*, vol. 43, no. 12, pp. 1462–1469, Dec. 2015, doi: 10.1016/j.jdent.2015.10.010.
[19] P. Carvalho *et al.*, “Influence of thickness and coatings morphology in the antimicrobial performance of zinc oxide coatings,” *Applied Surface Science*, vol. 307, pp. 548–557, Jul. 2014, doi: 10.1016/j.apsusc.2014.04.072.
[20] M. Visnapuu *et al.*, “UVA-induced antimicrobial activity of ZnO/Ag nanocomposite covered surfaces,” *Colloids and Surfaces B: Biointerfaces*, vol. 169, pp. 222–232, Sep. 2018, doi: 10.1016/j.colsurfb.2018.05.009.
[21] G. A. O’Toole and R. Kolter, “Initiation of biofilm formation in *Pseudomonas fluorescens* WCS365 proceeds via multiple, convergent signalling pathways: a genetic analysis,” *Molecular Microbiology*, vol. 28, no. 3, pp. 449–461, Apr. 1998, doi: 10.1046/j.1365-2958.1998.00797.x.
[22] J. Pasquet, Y. Chevalier, J. Pelletier, E. Couval, D. Bouvier, and M.-A. Bolzinger, “The contribution of zinc ions to the antimicrobial activity of zinc oxide,” *Colloids and Surfaces A: Physicochemical and Engineering Aspects*, vol. 457, pp. 263–274, Sep. 2014, doi: 10.1016/j.colsurfa.2014.05.057.
[23] R. Herrmann, F. J. García-García, and A. Reller, “Rapid degradation of zinc oxide nanoparticles by phosphate ions,” *Beilstein J. Nanotechnol.*, vol. 5, pp. 2007–2015, Nov. 2014, doi: 10.3762/bjnano.5.209.
[24] M. Li, L. Zhu, and D. Lin, “Toxicity of ZnO nanoparticles to Escherichia coli: mechanism and the influence of medium components,” *Environ. Sci. Technol.*, vol. 45, no. 5, pp. 1977–1983, Mar. 2011, doi: 10.1021/es102624t.
[25] R. Behra *et al.*, “Bioavailability of silver nanoparticles and ions: from a chemical and biochemical perspective,” *J R Soc Interface*, vol. 10, no. 87, p. 20130396, Oct. 2013, doi: 10.1098/rsif.2013.0396.
[26] Z.-M. Xiu, J. Ma, and P. J. J. Alvarez, “Differential effect of common ligands and molecular oxygen on antimicrobial activity of silver nanoparticles versus silver ions,” *Environ. Sci. Technol.*, vol. 45, no. 20, pp. 9003–9008, Oct. 2011, doi: 10.1021/es201918f.

[27] S. Suppi *et al.*, “A novel method for comparison of biocidal properties of nanomaterials to bacteria, yeasts and algae,” *Journal of Hazardous Materials*, vol. 286, pp. 75–84, Apr. 2015, doi: 10.1016/j.jhazmat.2014.12.027.
[28] J. T. Seil and T. J. Webster, “Reduced Staphylococcus aureus proliferation and biofilm formation on zinc oxide nanoparticle PVC composite surfaces,” *Acta Biomaterialia*, vol. 7, no. 6, pp. 2579–2584, Jun. 2011, doi: 10.1016/j.actbio.2011.03.018.
[29] R. Pati *et al.*, “Topical application of zinc oxide nanoparticles reduces bacterial skin infection in mice and exhibits antibacterial activity by inducing oxidative stress response and cell membrane disintegration in macrophages,” *Nanomedicine: Nanotechnology, Biology and Medicine*, vol. 10, no. 6, pp. 1195–1208, Aug. 2014, doi: 10.1016/j.nano.2014.02.012.
[30] J.-H. Lee, Y.-G. Kim, M. H. Cho, and J. Lee, “ZnO nanoparticles inhibit Pseudomonas aeruginosa biofilm formation and virulence factor production,” *Microbiological Research*, vol. 169, no. 12, pp. 888–896, Dec. 2014, doi: 10.1016/j.micres.2014.05.005.
[31] L. J. Lee, J. A. Barrett, and R. K. Poole, “Genome-wide transcriptional response of chemostat-cultured Escherichia coli to zinc,” *J. Bacteriol.*, vol. 187, no. 3, pp. 1124–1134, Feb. 2005, doi: 10.1128/JB.187.3.1124-1134.2005.
[32] B. Gómez-Gómez, L. Arregui, S. Serrano, A. Santos, T. Pérez-Corona, and Y. Madrid, “Unravelling mechanisms of bacterial quorum sensing disruption by metal-based nanoparticles,” *Science of The Total Environment*, vol. 696, p. 133869, Dec. 2019, doi: 10.1016/j.scitotenv.2019.133869.
[33] N. A. Al-Shabib *et al.*, “Biogenic synthesis of Zinc oxide nanostructures from Nigella sativa seed: Prospective role as food packaging material inhibiting broad-spectrum quorum sensing and biofilm,” *Sci Rep*, vol. 6, no. 1, p. 36761, Dec. 2016, doi: 10.1038/srep36761.
[34] B. García-Lara *et al.*, “Inhibition of quorum-sensing-dependent virulence factors and biofilm formation of clinical and environmental *Pseudomonas aeruginosa* strains by ZnO nanoparticles,” *Lett Appl Microbiol*, vol. 61, no. 3, pp. 299–305, Sep. 2015, doi: 10.1111/lam.12456.
[35] F. Zähringer, E. Lacanna, U. Jenal, T. Schirmer, and A. Boehm, “Structure and Signaling Mechanism of a Zinc-Sensory Diguanylate Cyclase,” *Structure*, vol. 21, no. 7, pp. 1149–1157, Jul. 2013, doi: 10.1016/j.str.2013.04.026.
[36] P. Stiefel, S. Schmidt-Emrich, K. Maniura-Weber, and Q. Ren, “Critical aspects of using bacterial cell viability assays with the fluorophores SYTO9 and propidium iodide,” *BMC Microbiology*, vol. 15, no. 1, p. 36, 2015, doi: 10.1186/s12866-015-0376-x.
[37] L. Brown, J. M. Wolf, R. Prados-Rosales, and A. Casadevall, “Through the wall: extracellular vesicles in Gram-positive bacteria, mycobacteria and fungi,” *Nat Rev Microbiol*, vol. 13, no. 10, pp. 620–630, Oct. 2015, doi: 10.1038/nrmicro3480.
[38] E.-Y. Lee *et al.*, “Gram-positive bacteria produce membrane vesicles: Proteomics-based characterization of Staphylococcus aureus-derived membrane vesicles,” *Proteomics*, vol. 9, no. 24, pp. 5425–5436, Dec. 2009, doi: 10.1002/pmic.200900338.
[39] F. Andreoni *et al.*, “Antibiotics Stimulate Formation of Vesicles in *Staphylococcus aureus* in both Phage-Dependent and -Independent Fashions and via Different Routes,” *Antimicrob Agents Chemother*, vol. 63, no. 2, pp. e01439-18, Dec. 2018, doi: 10.1128/AAC.01439-18.
[40] C. Formosa-Dague, P. Speziale, T. J. Foster, J. A. Geoghegan, and Y. F. Dufrêne, “Zinc-dependent mechanical properties of Staphylococcus aureus biofilm-forming surface protein SasG,” *Proc. Natl. Acad. Sci. U.S.A.*, vol. 113, no. 2, pp. 410–415, Jan. 2016, doi: 10.1073/pnas.1519265113.
[41] D. G. Conrady, C. C. Brescia, K. Horii, A. A. Weiss, D. J. Hassett, and A. B. Herr, “A zinc-dependent adhesion module is responsible for intercellular adhesion in staphylococcal biofilms,” *Proc. Natl. Acad. Sci. U.S.A.*, vol. 105, no. 49, pp. 19456–19461, Dec. 2008, doi: 10.1073/pnas.0807717105.
[42] K. Schwartz, A. K. Syed, R. E. Stephenson, A. H. Rickard, and B. R. Boles, “Functional amyloids composed of phenol soluble modulins stabilize Staphylococcus aureus biofilms,” *PLoS Pathog.*, vol. 8, no. 6, p. e1002744, 2012, doi: 10.1371/journal.ppat.1002744.

[43] M. M. Barnhart and M. R. Chapman, “Curli Biogenesis and Function,” *Annual Review of Microbiology*, vol. 60, no. 1, pp. 131–147, Oct. 2006, doi: 10.1146/annurev.micro.60.080805.142106.
[44] A. Taglialegna *et al.*, “Staphylococcal Bap Proteins Build Amyloid Scaffold Biofilm Matrices in Response to Environmental Signals,” *PLoS Pathog.*, vol. 12, no. 6, p. e1005711, 2016, doi: 10.1371/journal.ppat.1005711.
[45] A. Dutta, S. Bhattacharyya, A. Kundu, D. Dutta, and A. K. Das, “Macroscopic amyloid fiber formation by staphylococcal biofilm associated SuhB protein,” *Biophys. Chem.*, vol. 217, pp. 32–41, 2016, doi: 10.1016/j.bpc.2016.07.006.
[46] D. K. Ban and S. Paul, “Nano Zinc Oxide Inhibits Fibrillar Growth and Suppresses Cellular Toxicity of Lysozyme Amyloid,” *ACS Applied Materials & Interfaces*, vol. 8, no. 46, pp. 31587–31601, Nov. 2016, doi: 10.1021/acsami.6b11549.
[47] B. Ma, F. Zhang, X. Wang, and X. Zhu, “Investigating the inhibitory effects of zinc ions on amyloid fibril formation of hen egg-white lysozyme,” *International Journal of Biological Macromolecules*, vol. 98, pp. 717–722, May 2017, doi: 10.1016/j.ijbiomac.2017.01.128.
[48] A. Abelein, A. Gräslund, and J. Danielsson, “Zinc as chaperone-mimicking agent for retardation of amyloid β peptide fibril formation,” *Proceedings of the National Academy of Sciences*, vol. 112, no. 17, pp. 5407–5412, Apr. 2015, doi: 10.1073/pnas.1421961112.
[49] C. J. Sarell, S. R. Wilkinson, and J. H. Viles, “Substoichiometric Levels of Cu^{2+} Ions Accelerate the Kinetics of Fiber Formation and Promote Cell Toxicity of Amyloid-β from Alzheimer Disease,” *Journal of Biological Chemistry*, vol. 285, no. 53, pp. 41533–41540, Dec. 2010, doi: 10.1074/jbc.M110.171355.
[50] V. Tõugu *et al.*, “Zn(II)- and Cu(II)-induced non-fibrillar aggregates of amyloid-β (1-42) peptide are transformed to amyloid fibrils, both spontaneously and under the influence of metal chelators,” *Journal of Neurochemistry*, vol. 110, no. 6, pp. 1784–1795, Sep. 2009, doi: 10.1111/j.1471-4159.2009.06269.x.
[51] M. Slifkin and R. Cumbie, “Congo red as a fluorochrome for the rapid detection of fungi,” *J. Clin. Microbiol.*, vol. 26, no. 5, pp. 827–830, May 1988.
[52] P. N. Lipke, M. C. Garcia, D. Alsteens, C. B. Ramsook, S. A. Klotz, and Y. F. Dufrêne, “Strengthening relationships: amyloids create adhesion nanodomains in yeasts,” *Trends in Microbiology*, vol. 20, no. 2, pp. 59–65, Feb. 2012, doi: 10.1016/j.tim.2011.10.002.
[53] D. O. Serra, A. M. Richter, and R. Hengge, “Cellulose as an Architectural Element in Spatially Structured Escherichia coli Biofilms,” *Journal of Bacteriology*, vol. 195, no. 24, pp. 5540–5554, Dec. 2013, doi: 10.1128/JB.00946-13.
[54] P. Sudbery, N. Gow, and J. Berman, “The distinct morphogenic states of Candida albicans,” *Trends in Microbiology*, vol. 12, no. 7, pp. 317–324, Jul. 2004, doi: 10.1016/j.tim.2004.05.008.
[55] J. J. Harrison *et al.*, “Metal Ions May Suppress or Enhance Cellular Differentiation in Candida albicans and Candida tropicalis Biofilms,” *Applied and Environmental Microbiology*, vol. 73, no. 15, pp. 4940–4949, Aug. 2007, doi: 10.1128/AEM.02711-06.
[56] C. J. Nobile *et al.*, “Biofilm Matrix Regulation by Candida albicans Zap1,” *PLoS Biol*, vol. 7, no. 6, p. e1000133, Jun. 2009, doi: 10.1371/journal.pbio.1000133.
[57] S. Ganguly *et al.*, “Zap1 Control of Cell-Cell Signaling in Candida albicans Biofilms,” *Eukaryotic Cell*, vol. 10, no. 11, pp. 1448–1454, Nov. 2011, doi: 10.1128/EC.05196-11.
[58] C. J. Nobile and A. P. Mitchell, “Regulation of Cell-Surface Genes and Biofilm Formation by the C. albicans Transcription Factor Bcr1p,” *Current Biology*, vol. 15, no. 12, pp. 1150–1155, Jun. 2005, doi: 10.1016/j.cub.2005.05.047.
[59] D. Wilson, “Candida albicans,” *Trends in Microbiology*, vol. 27, no. 2, pp. 188–189, Feb. 2019, doi: 10.1016/j.tim.2018.10.010.
[60] S. Kurakado, R. Arai, and T. Sugita, “Association of the hypha-related protein Pra1 and zinc transporter Zrt1 with biofilm formation by the pathogenic yeast *Candida albicans*: Pra1 and Zrt1

regulate biofilm formation," *Microbiol Immunol*, vol. 62, no. 6, pp. 405–410, Jun. 2018, doi: 10.1111/1348-0421.12596.
[61] M. Cierech *et al.*, "Significance of polymethylmethacrylate (PMMA) modification by zinc oxide nanoparticles for fungal biofilm formation," *International Journal of Pharmaceutics*, vol. 510, no. 1, pp. 323–335, Aug. 2016, doi: 10.1016/j.ijpharm.2016.06.052.
[62] M. Jalal, M. A. Ansari, S. G. Ali, H. M. Khan, and S. Rehman, "Anticandidal activity of bioinspired ZnO NPs: effect on growth, cell morphology and key virulence attributes of *Candida* species," *Artificial Cells, Nanomedicine, and Biotechnology*, vol. 46, no. sup1, pp. 912–925, Oct. 2018, doi: 10.1080/21691401.2018.1439837.
[63] M. Divya *et al.*, "Biopolymer gelatin-coated zinc oxide nanoparticles showed high antibacterial, antibiofilm and anti-angiogenic activity," *Journal of Photochemistry and Photobiology B: Biology*, vol. 178, pp. 211–218, Jan. 2018, doi: 10.1016/j.jphotobiol.2017.11.008.
[64] K. Forsberg *et al.*, "*Candida auris* : The recent emergence of a multidrug-resistant fungal pathogen," *Medical Mycology*, vol. 57, no. 1, pp. 1–12, Jan. 2019, doi: 10.1093/mmy/myy054.
[65] P.-H. Lin, M. Sermersheim, H. Li, P. Lee, S. Steinberg, and J. Ma, "Zinc in Wound Healing Modulation," *Nutrients*, vol. 10, no. 1, p. 16, Dec. 2017, doi: 10.3390/nu10010016.
[66] I. Tenaud, S. Leroy, N. Chebassier, and B. Dreno, "Zinc, copper and manganese enhanced keratinocyte migration through a functional modulation of keratinocyte integrins," *Exp Dermatol*, vol. 9, no. 6, pp. 407–416, Dec. 2000, doi: 10.1034/j.1600-0625.2000.009006407.x.
[67] A. Chiba, S. Sugimoto, F. Sato, S. Hori, and Y. Mizunoe, "A refined technique for extraction of extracellular matrices from bacterial biofilms and its applicability: Extraction of ECM from bacterial biofilms," *Microbial Biotechnology*, vol. 8, no. 3, pp. 392–403, May 2015, doi: 10.1111/1751-7915.12155.

Funding & acknowledgements

We thank Arvo Tõnisoo for help with SEM imaging and Dr Nuno F. Azevedo for consulting on biofilms.

This work was supported by the Estonian Research Council grants IUT 23-5, PUT 748, EAG20, PRG749 European Regional Development Fund projects "Emerging orders in quantum and nanomaterials (TK134)" and "Advanced materials and high-technology devices for sustain-able energetics, sensorics and nanoelectronics (TK141)" and ERDF project Centre of Technologies and Investigations of Nanomaterials (NAMUR+, project number 2014-2020.4.01.16-0123).

Contributions

Merilin Rosenberg designed and executed biofilm experiments, analyzed the data and wrote the manuscript. Meeri Visnapuu designed and prepared the surfaces. Angela Ivask designed and executed the cell culture experiments, assisted in experimental design, participated in writing and amending the manuscript. Heiki Vija consulted on and executed elemental analysis. Kaja Kasemets consulted regarding yeast biology and assisted in writing the manuscript. Vambola Kisand designed the surfaces, assisted in experimental design, participated in writing and amending the manuscript. Anne Kahru consulted on general microbiology and critically edited the manuscript.

Competing Interests

The authors declare no competing interests.